Original Article

Institution of MECHANICAL ENGINEERS
Journal of AEROSPACE ENGINEERING

Proc IMechE Part G:
J Aerospace Engineering
2018, Vol. 232(15) 2745–2759

DOI: 10.1177/0954410017716193
journals.sagepub.com/home/pig
SAGE

Aero-structural optimization of shape memory alloy-based wing morphing via a class/shape transformation approach

Pedro BC Leal[1], Marcelo A Savi[2] and Darren J Hartl[1]

Abstract

Because of the continuous variability of the ambient environment, all aircraft would benefit from an in situ optimized wing. This paper proposes a method for preliminary design of feasible morphing wing configurations that provide benefits under disparate flight conditions but are also each structurally attainable via localized active shape change operations. The controlled reconfiguration is accomplished in a novel manner through the use of shape memory alloy embedded skin components. To address this coupled optimization problem, multiple sub-optimizations are required. In this work, the optimized cruise and landing airfoil configurations are determined in addition to the shape memory alloy actuator configuration required to morph between the two. Thus, three chained optimization problems are addressed via a common genetic algorithm. Each analysis-driven optimization considers the effects of both the deformable structure and the aerodynamic loading experienced by the wing. Aerodynamic considerations are addressed via a two-dimensional panel method and each airfoil shape is generated by the so-called class/shape transformation methodology. It is shown that structurally and aerodynamically feasible morphing of a modern high-performance sailplane wing produces a 22% decrease in weight and significantly increases stall angle of attack and lift at the same landing velocity when compared to a baseline design that employs traditional control surfaces.

Keywords

Shape memory alloys, multidisciplinary design optimization, airfoil parameterization, aircraft optimization

Date received: 10 February 2017; accepted: 26 May 2017

Introduction

The airfoil design associated with a given aircraft wing configuration is primarily intended to maximize performance during the predominant flight condition (e.g., cruise in transport aircraft) while generally considering constraints on performance in off-optimal conditions (e.g., during landing).[1] To overcome this performance loss, several methods exist to adapt the wing according to freestream conditions or changing performance requirements. The most common method is the inclusion of rigid but movable control surfaces, which permit the reconfiguration of the wing necessary to transition from takeoff to cruise to landing.[2] These mechanisms lead to higher performance during required maneuvers but are not without drawbacks. Due to their structural and mechanistic complexity, they occupy volume inside the wing, which might displace valuable fuel storage and clearly adds weight. Discontinuous surfaces also generate extra drag and noise at all flight conditions. These disadvantages motivate the use of alternative adaptive technologies, such as conformal wing morphing via implementation of shape memory alloys (SMAs) or other active materials.[3]

SMAs represent a class of materials that, when provided sufficient thermal energy, can generate a significant amount of actuation work in a monolithic and compact form requiring very little installation volume. Their actuation work density exceeds that attainable from all other current active material options.[4] Because of this, there has been a great interest in their use for aerospace applications[5] for the purposes of morphing or structural reconfiguration of air vehicles.

[1]Department of Aerospace Engineering, Texas A&M University, USA
[2]Department of Mechanical Engineering, Universidade Federal do Rio de Janeiro, Brazil

Corresponding author:
Darren J Hartl, Department of Aerospace Engineering, Texas A&M University, 3141 TAMU, College Station, TX 77843-3141, USA.
Email: darren.hartl@tamu.edu

In the literature, many works that address camber morphing mechanisms[6] incorporate solutions for alleviating strain in a morphed airfoil section such as rolling leading edge skin,[7] corrugated skins,[8–10] sliding skins,[11] and flexible skin.[12–17] The segmented concept herein presented requires none of these and remains smooth and continuous.[18] The implementation of an actuator that simultaneously enables smooth deformation is achieved through the use of SMAs. SMA components not only accommodate but actually induce the chord-wise axial strains in the skin needed for camber changes while preserving structural integrity and providing high stiffness.[5] Compared to other compliant skins, incorporating SMA actuators into the skin lowers interior volume requirements[9,13,15,16] and eliminates extra actuators for skin morphing.[13,14,17] Although SMAs are not energy efficient (around 10–15% efficiency[5]), the energy density is high (approximately 1200 J/kg) and the volumetric constraints for installation preclude the use of traditional actuators. Because of these advantages, there is great interest from the industry to implement this kind of alloy in several applications.[19]

There are many works considering the use of SMAs in a driving actuation mechanism. Due to the perceived limited variety of commercially available SMA forms, past works have focused primarily on the use of simple shapes, such as springs[20] and wires.[21,22] For applications such as camber morphing,[10,23,24] and SMA-driven control surfaces.[23,25,26] Regarding numerical analysis and especially design optimization of systems utilizing SMA actuators, relatively few papers exist. Strelec et al.[21] focused on the numerical and experimental use of nitinol (NiTi) wires to change the camber of an airfoil.[27] The work from Junior et al.,[28] the genesis of the current study, approximated the SMA transformation via artificial thermal expansive methods. Previous work demonstrated that SMA skin inserts are feasible as a solution for morphing from one National Advisory Committee for Aeronautics airfoil section to another. An aircraft utilizing this technology could morph the outer mold line (OML) while taking off or landing to improve aircraft performance. By locally heating an actuator formed using equiatomic SMA above approximately 100 °C, the structure can morph and change aerodynamic response. To avoid accidental actuation in extreme environmental conditions, higher temperature SMAs are being investigated.[29,30] In a previous flight test of a similar SMA application, heat was provided using surface-mounted resistive heaters.[19]

The goal of this paper is to expand the early efforts of Junior et al.,[28] where SMA inserts were embedded in the skin of the airfoil section and their size was optimized to drive morphing between two airfoil shapes. Here, the authors adopt the design process depicted in Figure 1, where aerodynamic effects are considered throughout the design process.[21] As in

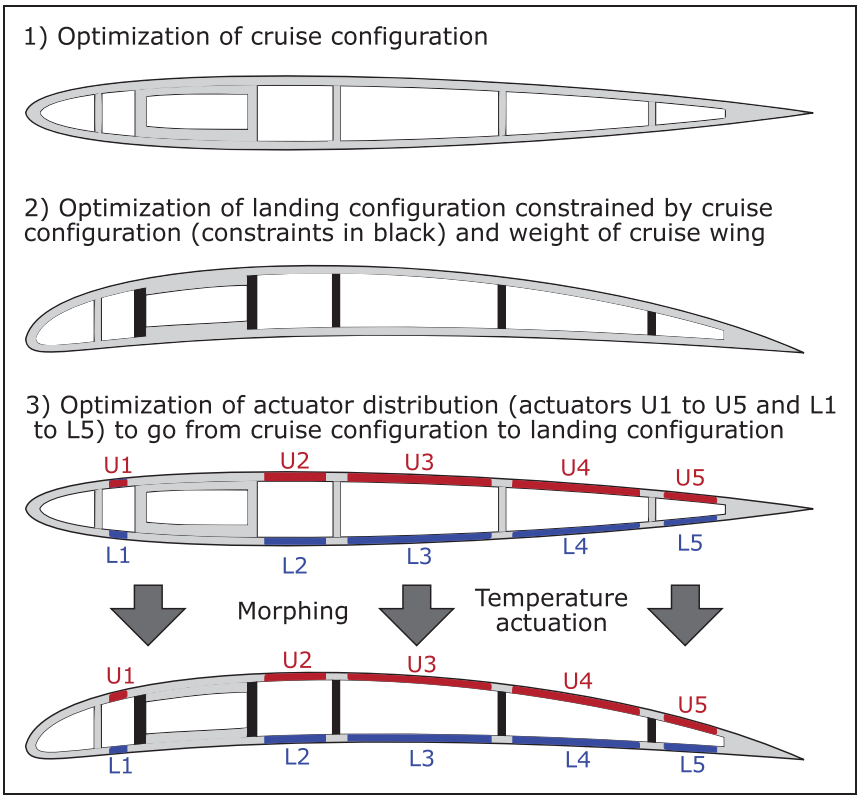

Figure 1. A high-level overview elucidating all the steps taken in this work.

Strelec et al.,[21] coupled fluid-structural effects are considered, and an accurate constitutive model describing the SMA material behavior is employed.[31] Novel herein are both the feasibility of the morphing approach and the method of airfoil section determination.[32] Instead of designing based on two arbitrarily chosen airfoils (as in the preliminary effort[28]), two custom-optimized airfoils are determined, each for a different flight condition. The shape of each independently optimized airfoil is described by the ''class/shape transformation'' methodology.[33] As shown in Figure 1, the OML of the cruise airfoil is first optimized given an assumed internal structural layout. The OML of the landing airfoil is then optimized given the constraints of the internal structure. Finally, an optimal actuation layout capable of morphing the airfoil between two target shapes is found. The overall optimization focuses on obtaining a wing with low weight, low drag at cruise, low landing velocity, and low bending displacement under lifting loads while providing sufficient lift and avoiding localized over-stress and buckling.

The remainder of this work is organized as follows. The main engineering design problem is proposed in section ''Engineering design problem.'' The engineering design tools utilized in this work are outlined in section ''Engineering design tools.'' The genetic optimization scheme, the class/shape transformation, and the fluid–structure interaction (FSI) framework utilized are thoroughly explained. The genetic optimization of the two discrete airfoil sections (cruise and landing) described via the class/shape transformation are presented in section ''Cruise and landing wing section optimization'' while a genetic optimization of the SMA actuators used to morph between the two airfoils is implemented in section ''Morphing optimization.'' Finally, section ''Conclusion'' summarizes the work and proposes future efforts.

Engineering design problem

The authors consider two key flight conditions:[34] cruise and landing. The considered wing is untapered and unswept to minimize three-dimensional effects during this assessment of the morphing and optimization approaches. Standard aluminum construction is also considered except where augmented via the placement of SMA actuation segments. The inner structure of the wing consists of an assembly of ribs, a spar, and a D-box.

For the first time, NiTi SMA inserts of various sizes are embedded in the skin of the airfoil section as depicted in Figure 1. Actuation (i.e., strain recovery) in these inserts is thermally induced so as to morph the wing from optimized cruise configuration to an optimized landing configuration and back again. The actuation deformations arising from the thermally induced phase transformation in these SMA inserts can generally be three dimensional, based on such aspects as local loading level, processing, and preparation. Here, it is considered that actuators comprising segments of the skin where all upper inserts are set to expand, and all bottom inserts are set to contract when activated. Ribs are not considered in the morphing model. The number of actuators is fixed at five based on previous work[28] and to maximize morphing capabilities; each actuator is placed at the midpoint between spars. It is considered that the ribs are structures having a tailored compliance; they carry transverse skin loads but do not hinder actuation capabilities.[8] Their detailed design will be assessed in future studies.

Engineering design tools

Because of the complexity of the adaptive aero-structural design problem in this work, several methods and existing software are utilized. Finite element analysis (FEA) considering deformation stress and buckling solutions is performed via Abaqus,[35] while the XFOIL[36] implementation of the panel method is used for estimating aerodynamic forces from a two-dimensional (2-D) flow perspective. An Abaqus user material subroutine is utilized to define the constitutive inelastic behavior of SMA.[37] Other important tools are described in this section. A custom-coded Python-scripted framework is used to integrate all tools into a single design framework.

Genetic optimization

Heuristic methods are more effective in finding global optima given a large number of design variables or highly non-linear or discontinuous design response. Therefore, the common robust genetic algorithm known as Non-dominating Sorting Genetic Algorithm II (NSGA-II)[38] is selected for all optimizations. This well-known option is included in the current distribution of NASA's Open-source Multidisciplinary Design Analysis and Optimization (OpenMDAO)[39] tool, the chosen Python framework for engineering analysis tool integration and optimization. In such a genetic scheme, each design variable is treated as a gene; a combination of these genes represents the chromosome of an individual design. Techniques inspired by natural evolution, including crossovers (80% probability of crossover of design variables and distribution index for crossover of 10), mutations (20% probability of mutation and distribution index for mutation of 50), and natural selection, generate a series of design population generations that should eventually include a nearly optimal solution.[38]

In general, NSGA-II can support n objective functions f_i (i.e., outputs of interest from our simulation such as lift or weight). Since the objective functions are of different orders of magnitude, normalization of each objective function f_i is

undertaken via the method proposed by Grodzevich and Romanko[40]

$$\bar{f}_i = \frac{f_i - f_i^U}{f_i^N - f_i^U} \quad \forall\, i = 1, \ldots, n \tag{1}$$

where f_i^U and f_i^N are, respectively, the *utopic* and *nadir* values of f_i. In the context of a minimization problem, the f_i^U is the minimum value possible and f_i^N is the maximum value expected given the bounds of the input variables. It suffices[40] for the purposes of normalization to select these values from a data set generated by a simple design of experiments (DOE).

In this work, a single cost function obtained via a normalized weight sum of the objective functions f_i[40] and the incorporation of constraints via the penalty method is used. This is because of the interest in identifying a single best design as opposed to a family of Pareto-optimal designs. Previous works demonstrated the capabilities of NSGA-II in single objective function problems.[41,42] Hence, if the objective function is subject to m equality constraints h and p inequality constraints g of the form

$$g_j \leqslant 0, \quad j = 1, \ldots, m \tag{2}$$

$$h_k = 0, \quad k = 1, \ldots, p \tag{3}$$

the cost function, C, for a multiobjective problem with n objective functions constrained via this penalty method is taken to be

$$C = \sum_{i=1}^{n} w_i \bar{f}_i + \sum_{j=1}^{m} \lambda_j^h \bar{h}_j + \sum_{k=1}^{p} \lambda_k^g \bar{g}_k \tag{4}$$

where w_i is the weight of each objective function that satisfies $\sum_i^k w_i = 1$, and λ^g and λ^h are Lagrange multipliers.

Class/shape transformation

The chosen method for generating the OML of the airfoil section is the class/shape transformation airfoil representation methodology.[33,43,44] Using a first-order Bernstein polynomial representation for the upper (u) and lower (l) airfoil surfaces gives

$$\begin{aligned} \xi_u &= \psi^{0.5}(1-\psi)[A_{u_0}(1-\psi) + A_{u_1}\psi] + \psi\frac{\Delta\xi_{TE}}{2} \\ \xi_l &= \psi^{0.5}(\psi-1)[A_{l_0}(1-\psi) + A_{l_1}\psi] - \psi\frac{\Delta\xi_{TE}}{2} \end{aligned} \tag{5}$$

where ψ and ξ are the normalized distances along the chord line and perpendicular to it, respectively; A_{u_0}, A_{u_1}, A_{l_0}, and A_{l_1} are the Bernstein polynomial coefficients (unbounded); and $\Delta\xi_{TE} \geqslant 0$ is the normalized trailing edge thickness. The Bernstein polynomial coefficients are taken to be initially unknown and must be determined by the optimization process. Figure 2 clarifies the $\xi - \psi$ space and depicts the influence of each coefficient over the shape obtained using equation (5).

In this paper, the OML shapes of the cruise and landing airfoil sections are of interest. The distances to the upper and lower surfaces perpendicular to the chord line for cruise are denoted by ξ_u^C and ξ_l^C, respectively, while for landing they are denoted by ξ_u^L and ξ_l^L. Due to the morphing wing design concept of Figure 1 and, in particular, the existence of the fixed spars/longerons, extra design constraints related to thicknesses of the airfoil section (i.e., the distance between upper and lower surface) are considered. The airfoil thicknesses are necessary to constrain possible landing configurations to feasible OMLs. To implement this constraint, the airfoil thickness at four points along the chord (ψ_1, ψ_2, ψ_3, and ψ_4), once determined for an optimized cruise configuration, is imposed on the shape equation defining the airfoil optimized for landing. The functions $\{\xi_u^L, \xi_l^L\}$ then depend only on $\{\xi_u^C, \xi_l^C\}$. This enables static spar geometries and thus use of the proposed skin-based morphing approach while still allowing great freedom in the landing shape design. Using $\Delta\xi_i$ to denote known differences between the upper and lower surfaces (i.e., airfoil thickness) at ψ_i

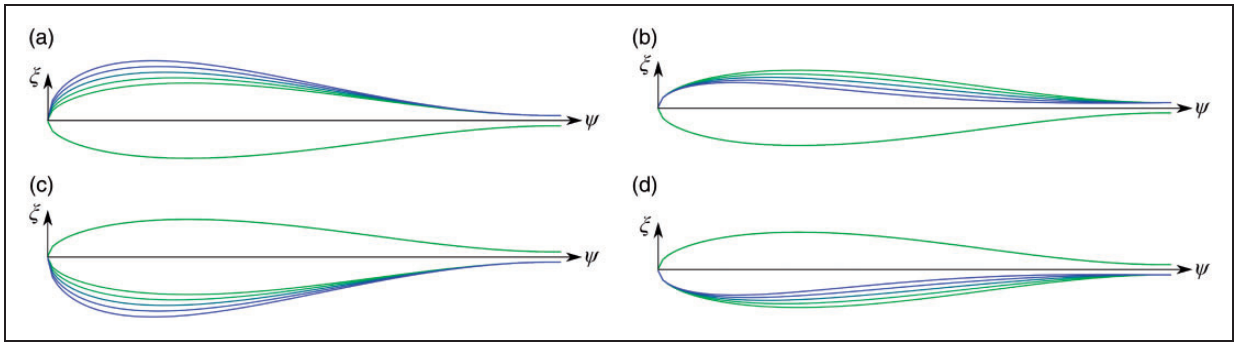

Figure 2. Influence of each of the Bernstein polynomial coefficients over airfoil section geometric properties. (a) A_{u_0} (forward thickness, upper skin); (b) A_{u_1} (afterward thickness, upper skin); (c) A_{l_0} (forward thickness, lower skin); and (d) A_{l_1} (afterward thickness, lower skin).

$\left(\Delta\xi_i = \xi_u^C(\psi_i) - \xi_l^C(\psi_i)\right)$ at each point $i = 1, \ldots, 4$, from system of equations (5)

$$A_{u_0} = \frac{K_2\psi_1 - K_1\psi_2}{\psi_1 - \psi_2} - A_{l_0}$$
$$A_{u_1} = \frac{K_1(1-\psi_2) + K_2(\psi_1 - 1)}{\psi_1 - \psi_2} - A_{l_1} \qquad (6)$$
$$\text{where, } K_i = \frac{\Delta\xi_i - \psi_i\Delta\xi_{TE}}{\psi_i^{0.5}(1-\psi_i)}$$

For the landing optimization, the airfoil thicknesses $\Delta\xi_i$ at positions ψ_i, $i = 1 \ldots 4$ are known from the cruise airfoil; hence, the total number of unknowns across the two equations is reduced to two, A_{l_0} and A_{l_1}, given that $A_{u_0} = f(\psi_1, \psi_2, A_{l_0}, \Delta\xi_1, \Delta\xi_2)$ and $A_{u_1} = f(\psi_3, \psi_4, A_{l_1}, \Delta\xi_3, \Delta\xi_4)$. In this way, the number of design variables for the landing airfoil design case is reduced, while the structural feasibility of the morphing structure design (i.e., the integrity of non-morphing internal components) is guaranteed.

Fluid–structure interaction

Coupled aero-structural response is considered for the optimization of the morphing wing presented in this work. The approach for computing the response of this coupled mechanical system follows from that of Felippa et al.[45] The computational multiphysics framework utilized[46] is developed for a staggered solution problem using two differential partitions. An overview of the staggered solution considered is depicted in Figure 3. The staggered representation then enables the utilization of non-matching spatial discretizations and geometric representations, which is a requirement for efficient calculation of aerodynamic effects via the panel method. For computational treatment of a coupled system such as an aero-structural simulation, the decomposed systems are the fluid and solid domains, where the solid domain is volumetrically discretized, the panel method model discretizes the surface comprising of the airfoil section contour, and field solutions are determined over each. At each time interval, further decomposition of the time discretization of only one of the two fields is possible; this approach is known as *splitting* or *subcycling*.[45] In the finite element model, this feature is of importance given numerical stability challenges associated with large deformations and non-linear materials.

In the context of this current effort, the developed framework allows the calculated pressure distribution to update based on the calculated deformed airfoil shape, while the aero-structural loads likewise update based on changing pressures. This occurs throughout a dynamic analysis. Information regarding the OML of the Abaqus model is transferred to XFOIL via a custom-coded Python interface called AeroPy,[47] where the pressure distributions are calculated and then transferred back to Abaqus. XFOIL utilizes a e^N method for transition prediction. A value of $N = 12$, equivalent of a 0.02% turbulence level, is an appropriate value for a glider;[36] thus, it is utilized. All other parameters such as trip position and initial transitions constants are the default for XFOIL. The incremental process repeats itself in this explicit manner until the total simulated time has been reached. For morphing, it is assumed that the physical process is relatively slow (i.e., quasi-static) and that the flow has sufficient time to stabilize between each morphing increment; therefore, the panel method analysis provides only steady-state solutions at each increment. Figure 3 represents the coupled aero-structural morphing framework used in section "Morphing optimization." In section "Cruise and landing wing section optimization," the full FSI framework is not used; rather, at the beginning of each simulation the aerodynamic loads are calculated via the panel method and then imposed on the FEA structural model.

Figure 4 summarizes the full engineering design problem in section "Engineering design problem" and the tools of section "Engineering design tools." As illustrated, the three optimization problems being considered are coupled in the following way: (1) the optimized values for the airfoil thicknesses and number of ribs determined via cruise analysis are passed as inputs into the landing analysis, (2) restrictions regarding the spars and stiffeners utilizing the

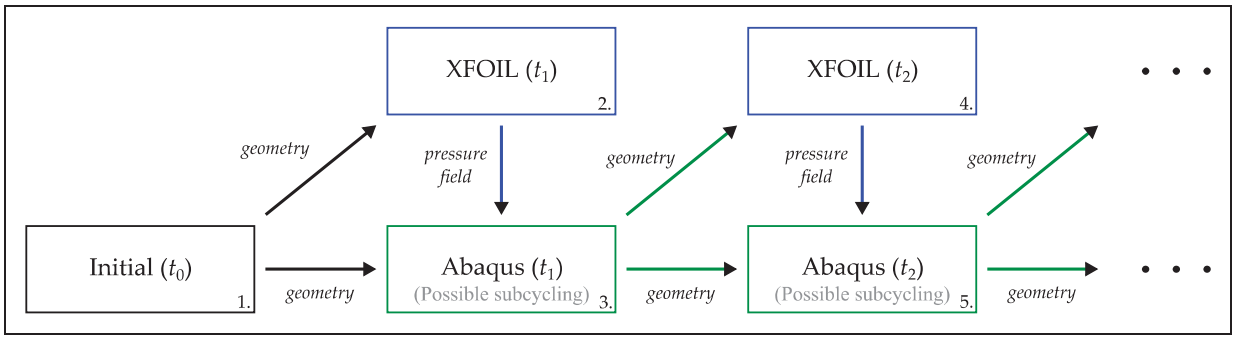

Figure 3. Flowchart of the fluid–structure simulation used for the morphing optimization.

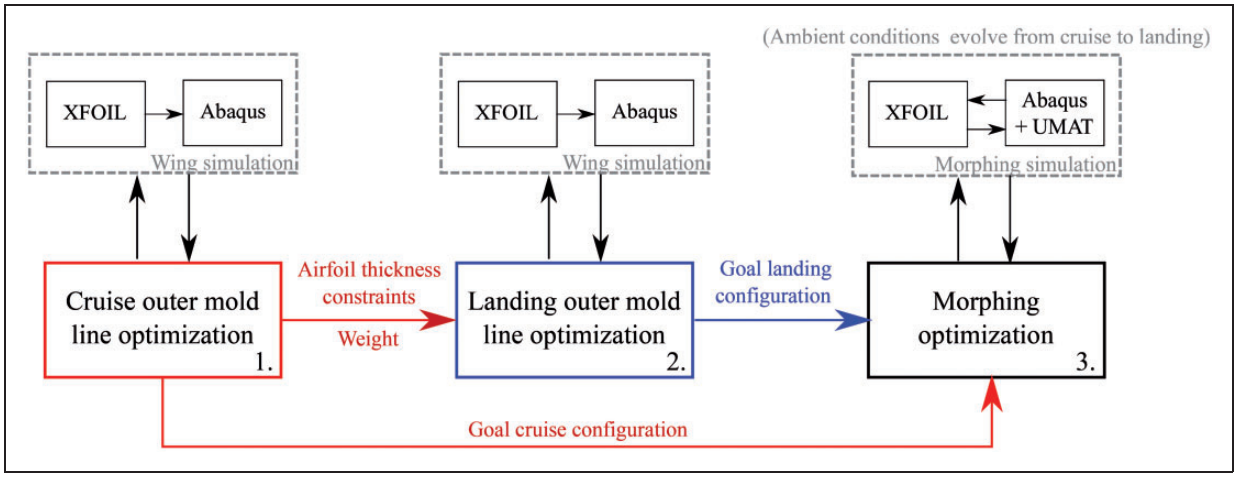

Figure 4. Flowchart describing the overall coupled design problem and associated approach considered (cf. Figure 1).

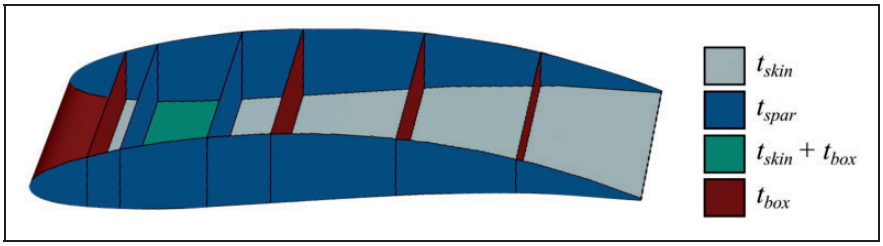

Figure 5. An example wing bay of the shell model near the fuselage.

parameters $\{\psi_1, \psi_2, \psi_3, \psi_4\}$ and $\{\Delta\xi_1, \Delta\xi_2, \Delta\xi_3, \Delta\xi_4\}$ calculated for cruise are imposed on landing configurations as mentioned in Class/shape transformation and (3) the results obtained from both optimizations are used for morphing in section "Morphing optimization".

Cruise and landing wing section optimization

To begin, steps 1 and 2 of Figure 4 are addressed in this section. The model and cost functions utilized for solving each step are stated and developed. Analysis of the influence of the design variables and the optimization of each problem are also undertaken.

Engineering design problem

In the wing model considered (cf. Figure 5), different thicknesses are assumed for several components while the number of ribs is fixed to 19. The thicknesses of the *inner* components (spars, skin, and D-box) are t_{spar}, t_{skin}, and t_{box}. The thickness of rib components is the same as it is for spars. Figure 5 depicts how the thickness is assigned throughout the wing. Desired values for each thickness and the shape variables (A_{l_0}, A_{l_1}, A_{u_0}, and A_{u_1}) are found via the cruise optimization (step 1). The upper aluminum components of the wing are modeled as AL-2024-T3 and the lower components as AL-7075-T6. The properties of both alloys are taken to be dependent on local component thickness.[48] The SMA inserts are conservatively assumed to be of maximum length, where the SMA properties are given by Saunders et al.[49] Other parameters that are held constant throughout analysis and optimization are: the weight of the aircraft excluding the wings (1000 N), wing chord of 1.0 m, aircraft wing span of 20 m, drag coefficient for the fuselage of 0.3, fuselage cross section area of 0.18 m^2, and a trailing edge thickness $\Delta\xi_{TE}$ equal to 4 $\dot{m}m$.[50] Although this study is hypothetical in nature, the optimal cruise wing is compared to a modern high-performance two-seat sailplane, the ICA IS-32 produced by Industria Aeronautică Română Brasov,[51] to place these results in the context of a real-world aircraft. This Romanian sailplane has the equivalent wing span of the aircraft modeled and is also of all-metal construction, thereby rendering it a reasonable choice for assessing feasibility. The selected cruise velocity of 30 m/s (59 ft/s) is similar to the best glide velocity of the ICA IS-32.[51] Other relevant properties of the Romanian glider are an aspect ratio of 27.25 and a maximum weight of 5900 N.

The first optimization is initiated with the creation of random wing design configurations as depicted in the cruise airfoil design flowchart of Figure 6. For each configuration, an Abaqus structural model of the entire wing is created and the total aircraft weight is calculated. The minimal cruise angle of

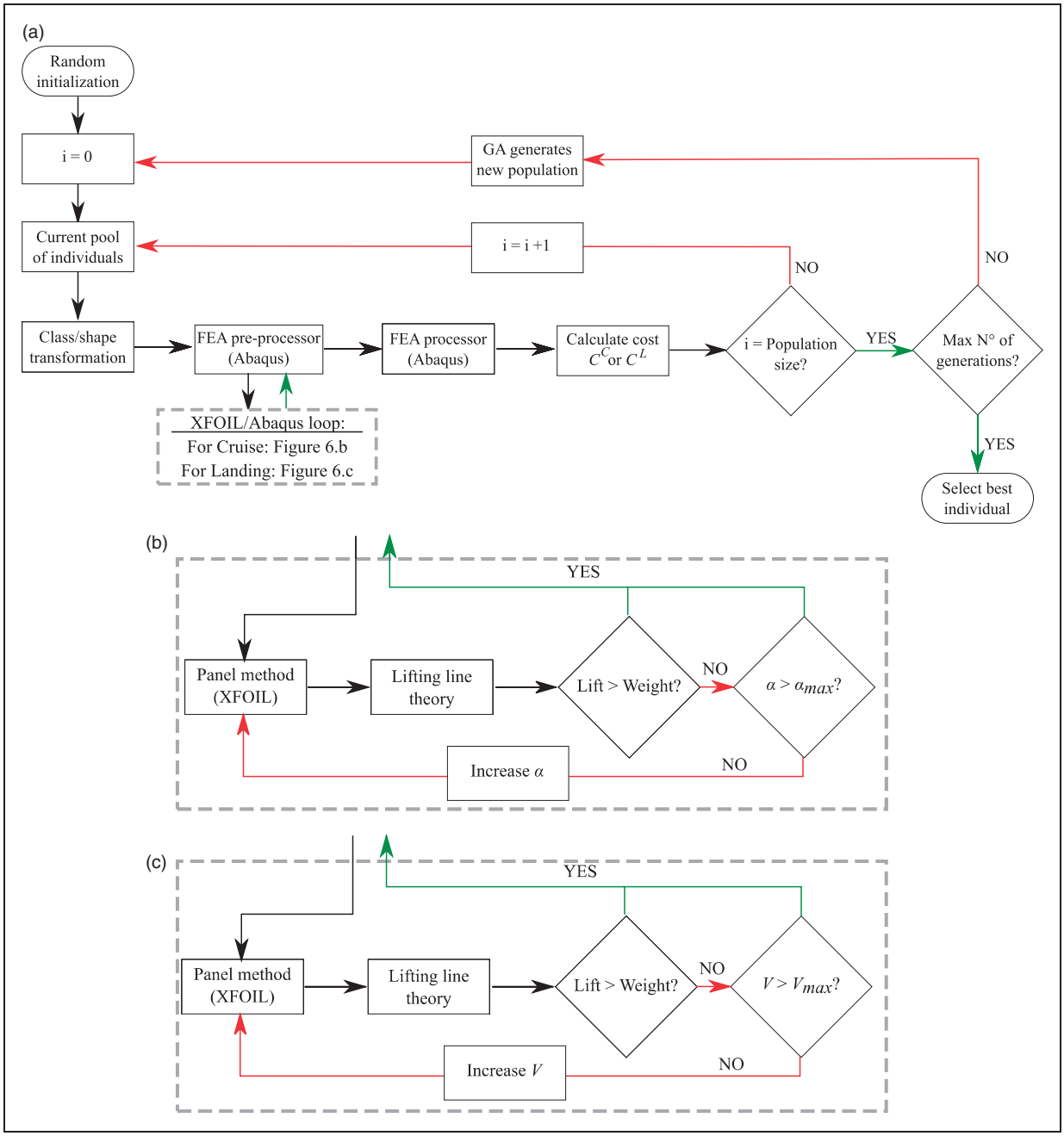

Figure 6. Flowchart of the airfoil shape optimization for cruise and landing. (a) Flowchart of the airfoil shape optimization common for both flight conditions (cruise and landing); (b) XFOIL/Abaqus loop for cruise; and (c) XFOIL/Abaqus loop for landing.

attack at the root α^C, that provides sufficient lift, if it exists, is found via XFOIL and the classical Prandtl lifting line theory[2] for a fixed cruise velocity. 2-D pressure distributions are calculated via XFOIL for α^C at the root for the angle of attack that generates zero lift for the airfoil selected, and for all the local induced angles of attack along the wingspan; the three-dimensional (i.e., full wing) loads are then computed via the lifting line theory. The loads are then passed into Abaqus via Python scripts and FEA is completed. If the wing is found to violate structural constraints on local stress limits, the configuration is penalized as described in optimization cost function. The same penalty is applied if the structure is predicted to buckle (i.e., the *buckling eigenvalue* is smaller than one).[35] If the maximum number of genetic algorithm generations has not been reached, a new generation is created according to the NSGA-II algorithm based on drag and weight metrics. Otherwise, the best configuration among all members of the design populations of all generations is assumed to best approximate the optimal design. For landing, the same process is applied, but the minimum aircraft velocity necessary for landing (i.e., as calculated from XFOIL; lift equal to weight) is assessed instead of the minimum angle of attack at the root.

The optimized landing and cruise airfoil sections must inherently have equal mass. However, strict

Table 1. Wing design problem definition.[AQ: Please check whether the tables are correct as set.]

	Cruise configuration	Landing configuration
Minimize:	Drag (D) Weight (W)	Velocity (V) Weight difference (ΔW)
By varying inputs:	A_{l_0}, A_{l_1}, A_{u_0}, A_{u_1} t_{span}, t_{box}, t_{skin}	A_{l_0} and A_{l_1}
Subject to constraints:	Wing tip displacement < 1 m	
	Aluminum maximum von Mises stress < aluminum yield stress	
	SMA maximum von Mises stress < SMA yield stress	
	Lift (L) equal to weight (W)	
	No localized buckling	

SMA: shape memory alloy.

satisfaction of this design requirement via a directly imposed constraint was found to be too restrictive to the optimization process since each section is independently optimized. Rather, the difference between landing and cruise wing weights is a constraint to be satisfied at least approximately via penalties in the objective functions. Table 1 summarizes the wing design problem described.

Optimization cost function

The wing design problem for each flight condition considers two objective functions, three inequality constraints (buckling, von Mises stress, and wing tip displacement limits), and one equality constraint (lift equal to weight). Instead of eliminating designs predicted to violate these constraints outright, it is more conducive to the optimization that these individuals be penalized instead. Therefore, configurations near the global minimum that violate the constraints by a small margin may not be eliminated from the population. Normalizing each output according to equation (1) using data, regarding minimums and maximums obtained from the design of experiments, the scalar cost functions (equation (4)) for cruise and landing (C^C and C^L, respectively) are given as

$$C^C = w_D \frac{D-125.2}{486.7} + w_W \frac{W-4247.1}{9825.11} + \lambda\left(\frac{L-W}{13457} + \langle v-1\rangle + \left\langle\frac{\sigma_{VM}-\sigma_y}{\sigma_y}\right\rangle + \langle u-1\rangle\right) \tag{7}$$

$$C^L = w_V \frac{V-14.03}{12.05} + w_{\Delta W} \frac{\Delta W-56.01}{38.18} + \lambda\left(\frac{L-W}{10363.32} + \langle v-1\rangle + \left\langle\frac{\sigma_{VM}-\sigma_y}{\sigma_y}\right\rangle + \langle u-1\rangle\right) \tag{8}$$

where w_D, w_W, w_V, and $w_{\Delta W}$ are, respectively, the weighting factors for drag (D), aircraft weight (W), velocity (V), and weight difference (ΔW). Also, v is the buckling eigenvalue, σ_{VM} is the maximum von Mises stress, σ_y is the aluminum yield stress, and u is the wing tip displacement. The inequality constraints only apply when they are violated, hence the Macaulay brackets[52] ($\langle\cdot\rangle$). The weighting factors are determined based on prior simulations, and it has been determined through trial and error that w_D, w_W, w_V, and $w_{\Delta W}$ should be 0.7, 0.3, 0.8, and 0.2. The weights were empirically determined by the authors to give priority to certain objectives (drag and velocity) while still minimizing secondary objectives (weight and weight difference). Because all the components related to a constraint are also normalized, only one penalty factor is herein utilized. The penalty factor λ is equal to 10^n, where at the first generation $n=-1$ and every five generations, n is increased by one for the purpose of increasing penalization as the population evolves. Due to the highly constrained nature of the cruise optimization problem, it was initially observed that a strict enforcement of stress and buckling limits led to insufficient diversity in the initial generations of the genetic algorithm search. Relaxed enforcement in initial generations enables greater flexibility to explore the design domain. An increasing penalty factor approach was chosen after Bryan and Shibberu[53] as a means to ensure the strict feasibility of designs in the final generation.

Since the constraints are taken into consideration via the cost function, the two reformulated *unconstrained* problems are summarized in Table 2 considering the DOE results.

Results

The majority of airfoils from Abbott and von Doenhoff[54] exhibit lift responses that deviate from linear only at angles of attack higher than 10°. It is assumed that the optimized landing airfoil will have an enhanced performance than more traditional airfoils. Consequently, a 10° angle of attack is considered high enough for landing. The approximated optimum design variables obtained for both optimizations are given in Table 3 and key output variable results through 20 generations, each with a population of 60 individuals, can be seen in Figure 7. The running time for each

Table 2. Reformulated unconstrained cruise and landing wing design optimization problems.

	Cruise configuration	Landing configuration
Minimize:	C^C (equation (7))	C^L (equation (8))
By varying inputs:	$0.1 \leqslant A_{l_0} \leqslant 0.3$	$0.05 \leqslant A_{l_0} \leqslant 0.15$
	$-0.15 \leqslant A_{l_1} \leqslant 0.2$	$-0.3 \leqslant A_{l_1} \leqslant 0.05$
	$0.16 \leqslant A_{u_0} \leqslant 0.4$	
	$0.16 \leqslant A_{u_1} \leqslant 0.4$	
	2 mm $\leqslant$ spar thickness (t_{spar}) $\leqslant$ 10 mm	
	4 mm $\leqslant$ box thickness (t_{box}) $\leqslant$ 20 mm	
	0.2 mm $\leqslant$ skin thickness (t_{skin}) $\leqslant$ 8 mm	

Table 3. Estimated optimized design variables and structural/aerodynamic properties for landing and cruise sections.

	Variables	Cruise section	Landing section
Inputs	t_{spar} (mm)	6.8	–
	t_{skin} (mm)	1.8	–
	t_{box} (mm)	6.1	–
	A_{u_0}	0.1805	0.2694
	A_{u_1}	0.1622	0.3001
	A_{l_0}	0.1184	0.0733
	A_{l_1}	−0.0959	−0.2776
Outputs	Weight (N)	4594.7	4669.8
	Lift (N)	4594.6	4667.8
	Drag (N)	105.8	188.1
	Wingtip Disp. (m)	0.5	0.34
	Eigenvalue	2.64	3.6
	Max von Mises (MPa)	75.3	59.5
	Angle of attack (°)	2	10 (given)
	Velocity (m/s)	30 (given)	15

optimization is approximately 36 h. While for some NSGA-II optimizations it may be possible to find the global optimum with a small population,[55] here the authors claim only to obtain an estimate of the global optimums for both problems. Particularly for cruise, there are configurations with low drag and weight that severely violate the equality and inequality constraints. The final result represents the best feasible solution.

Aerodynamic and structural performance outputs of the two approximately optimized airfoils are given in Table 3. The gross weight of the optimized wing is 22% lower in comparison to the IS-32 (5900 N), but the calculated L/D for cruise (43.4) is slightly worse than that given for the ICA IS-32 ($L/D = 44.5$). Therefore, the approximated optimized morphing aircraft is lighter than its real-world counterpart, but it is approximated via 2-D panel methods and lifting line theory to be less efficient at cruise. As desired, the higher camber landing airfoil allows a lower landing velocity of 15 m/s without the need for discrete flaps, which is 50% of the cruise velocity. A geometric comparison of the optimized sections is seen in Figure 8, where the *shape difference* for a given coordinate ψ is simply calculated as $\left|\left[\xi_u^C(\psi) - \xi_l^C(\psi)\right] - \left[\xi_u^L(\psi) - \xi_l^L(\psi)\right]\right|$. Comparing the two airfoil shapes in the figure, it is noticeable that the moment of area for the landing airfoil is higher than the cruise airfoil; hence, the wingtip displacement and maximum von Mises stress for landing are 24% and 21% smaller than for cruise, respectively.

The ICA IS-32 uses an FX 67-K-150/17 airfoil;[51] XFOIL analysis performed on such a wing section at landing velocity without taking into consideration the effects of the fuselage over weight and drag provides a baseline to which the two optimized airfoils can be compared. The maximum lift-over-drag for the FX 67-K-150/17 ($L/D = 141.6$) is higher than for the optimized airfoils for landing ($L/D = 131.6$) and cruise ($L/D = 96.9$). However, the landing and cruise airfoils are predicted to stall later and generate more lift at the landing angle of attack (for cruise $c_L = 1.552$ and for landing $c_L = 1.308$) than the FX 67-K-150/17 ($c_L = 1.014$). Moreover, the optimized total aircraft weight is considerably smaller than the baseline, thus less lift is necessary. Overall, the lift and drag of the optimized aircraft are roughly equal to the reference sailplane. This is considered sufficient for validating the efficacy of our current approach in a preliminary sense. It is essential to recognize, however, that the theoretical designed wing is capable of high performance in *both* landing and cruise due to the novel SMA-based morphing capability, the design of which is described in the following section.

Morphing optimization

While the optimization of multiple fixed-point wing designs for various flight conditions is in itself an interesting goal, the main objective of this paper is to study the use of SMA components as a means to morph *between* discrete optimized shapes. This more difficult design task is described in this section.

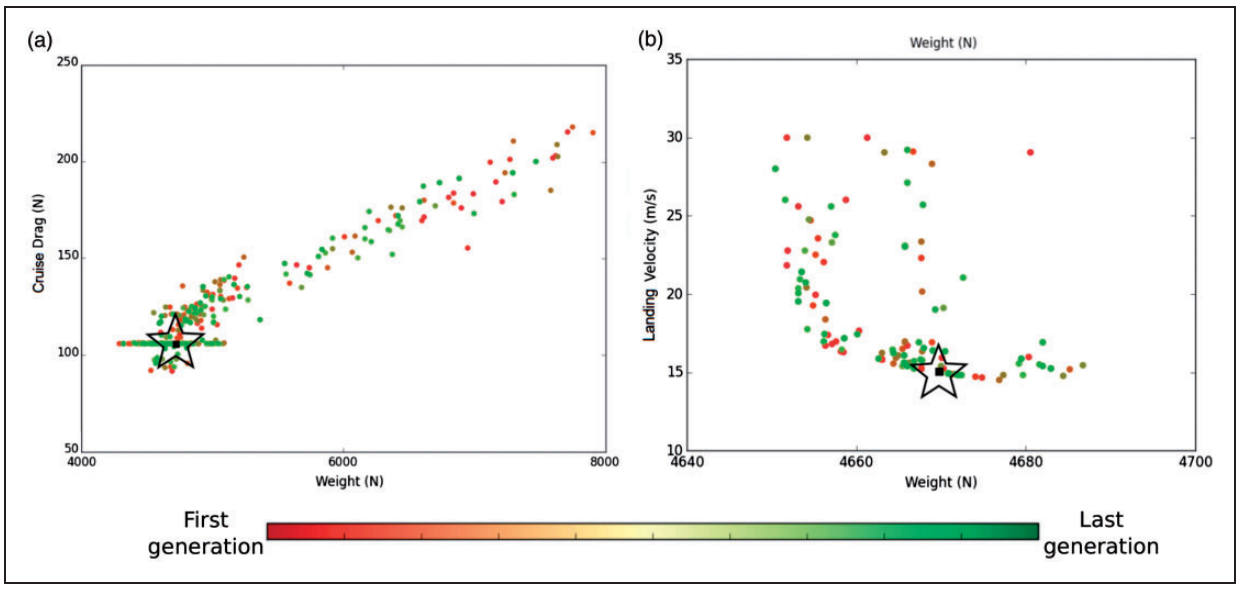

Figure 7. Plots of the design domain for both problems. Best solutions are highlighted by a star. The total amount of generations is 20. (a) Cruise optimization and (b) landing optimization.

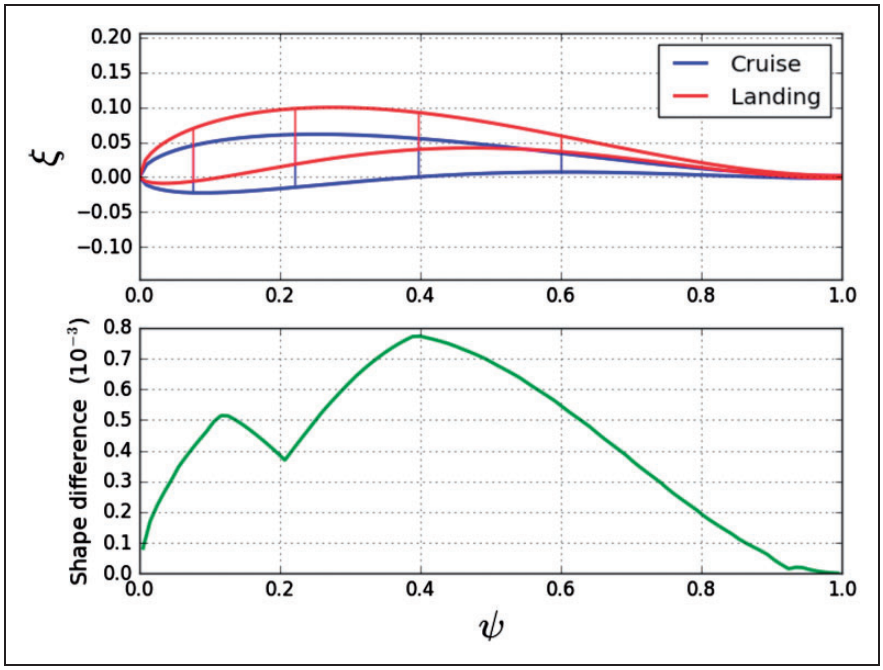

Figure 8. Optimized airfoil section profiles and the shape difference. The sections with constant airfoil thickness are depicted.

Design optimization problem

Because the wing sections and internal configuration for cruise and landing have already been optimized, the only design variables to be considered during morphing optimization are the widths of each insert of the 2-D model labeled in Figure 1. The morphing optimization scheme is similar to that used previously for finding the landing and cruise airfoil sections, though no equality constraint with respect to the lift and weight is considered. During the cruise and landing optimizations, the SMA inserts were assumed at maximum width; the widths actually required for morphing are expected to be smaller. The effects of substituting SMA material for structural aluminum reduce the weight and modify the structural performance slightly, but for the better since the structure is subject to smaller stresses. These effects are conservatively neglected. The objective of the SMA actuators is to morph a wing with an OML designed for cruise into a wing designed for landing. Once again, the optimization process leverages the integrative capabilities and built-in optimization algorithms of OpenMDAO.

The properties of the SMA inserts are taken from prior research efforts.[49]

During the FSI simulation of the morphing problem, the altitude and velocity of the aircraft are evolved, hence the freestream fluid conditions are updated at each time interval of the FSI. Through the ideal gas assumption and Sutherland's law, the freestream fluid temperature (T_{air}), pressure (P_{air}), dynamic viscosity (μ_{air}), and density (ρ_{air}) in the troposphere[56] (altitude $\lesssim 12\,km$) are calculated.

The morphing process is a slow adaptive procedure occurring during landing. The evolving state variables used to simulate the landing transition (as first described in fluid-structure interaction) are smoothly modified.[35] The transition between both altitudes occurs over 700 s, where aircraft altitude is smoothly decreased[35] from 3048 m (10,000 ft) to 305 m (1000 ft). The angle of attack, freestream fluid conditions, and freestream velocity are smoothly altered in phase to simulate the landing transition as mentioned in fluid-structure interaction. The initial and final velocities, altitude, and angle of attack are the same as those determined in the previous section for cruise and landing. To initialize the analysis, the flow is accelerated over 1 s from zero to the cruise velocity and the SMA insert temperature is increased from 342 K up to 370 K for the next 99 s with constant flight conditions. For the next 600 s, the SMA inserts continue to be heated while the aircraft altitude and angle of attack change from cruise to landing conditions. The temperature increase causes actuation of the SMA inserts and the shape of the airfoil is modified. In the final phase (100 s), the SMA temperature is held constant and landing conditions are finally achieved.

The main objective of the optimization is to obtain a morphed airfoil structure that is approximately equivalent to the optimized landing airfoil; hence, the optimization minimizes the shape difference between morphed and goal landing sections by varying the SMA insert lengths. The wing must maintain structural integrity even when fully actuated and feasible designs cannot buckle or plastically deform. The morphing optimization problem is summarized in Table 4.

Table 4. Morphing optimization problem.

Minimize:	Shape difference between morphed and goal landing sections
By varying inputs:	l_{U1}, l_{U2}, l_{U3}, l_{U4}, l_{U5}, l_{L1}, l_{L2}, l_{L3}, l_{L4}, and l_{L5}
Subject to constraints:	Aluminum max. von Mises stress $<$ aluminum yield stress
	SMA max. von Mises stress $<$ SMA yield stress
	No buckling

SMA: shape memory alloy.

Cost function

Using the cruise airfoil as a known reference configuration, the cost function for the morphing design optimization is based on shape morphing error computed as the sum of the differences between the nodal positions at the outer contour of a given trial-morphed design as compared to those of the goal *landing* airfoil section (Figure 8, where the error function is first introduced) as described by Junior.[28] To calculate this error, a Python script is developed to: (i) identify the trailing and leading edges of the goal and analysis-generated airfoils, (ii) position both airfoils so that the trailing edges overlap and the chords are aligned, and (iii) calculate the difference between node positions of the two airfoil surfaces. In the general case that the nodes do not match to within some tolerance, linear interpolations are implemented. The cost function then penalizes morphing designs (i.e., SMA insert configurations) resulting in non-matching chords or wings that buckle or exhibit unreasonably high stresses. Following the general form of equation (4), the following cost function for the morphing optimization is used

$$C^M = \sum_{i=1}^{N-1} \left| \left(\psi_i^M - \psi_{i+1}^M\right)\left(\frac{\xi_i^M + \xi_{i+1}^M}{2} - \xi_i^{goal}\right)\right| + \lambda\left(\langle \nu - 1\rangle + \left\langle \frac{\sigma_{VM} - \sigma_y}{\sigma_y}\right\rangle\right) \tag{9}$$

where N is the number of nodal points comprising the OML of the finite element model, $|\cdot|$ indicates an absolute value, ψ^M and ξ^M are the ψ and ξ coordinates of the ith point of the morphed finite element model outer mold (see section 3.3.2 for definition of ξ and ψ), ξ^{goal} is the ξ coordinate of the goal landing outer mold calculated in section "Cruise and landing wing section optimization" and the other variables (λ, ν, $\sigma_{V\,M,}$ and σ_y) are the same as in previous suboptimization. The morphing design optimization problem utilizing the cost function from equation (9) is summarized in Table 5.

Results

An optimal design is approximated using the iterative process for 12 generations with a population size of 20

Table 5. Morphing optimization problem.

Minimize:	Shape difference between morphed and goal landing sections (equation (9))	
By varying inputs:	$10\,mm \leqslant l_{U1} \leqslant 30$ mm	$10\,mm \leqslant l_{U2} \leqslant 90$ mm
	$10\,mm \leqslant l_{U3} \leqslant 90$ mm	$10\,mm \leqslant l_{U4} \leqslant 90$ mm
	$10\,mm \leqslant l_{U5} \leqslant 20$ mm	$10\,mm \leqslant l_{L1} \leqslant 30$ mm
	$10\,mm \leqslant l_{L2} \leqslant 90$ mm	$10\,mm \leqslant l_{L3} \leqslant 90$ mm
	$10\,mm \leqslant l_{L4} \leqslant 90$ mm	$10\,mm \leqslant l_{L5} \leqslant 20$ mm

individuals per generation. Each of the 240 FSI analyses took 14 min to complete, for a total optimization time of 56 h. The best SMA inserts widths after 12 generations are given in Table 6, where the variables correspond to the labels in Figure 1.

As seen in Figure 9, actuation of appropriately optimized SMA inserts results in an OML similar to, but not identical to, the goal OML.

The airfoil thickness constraints established in system of equations (6) are introduced to ensure rigid component (spars and stringers) dimensions are maintained. However, such constraints seem to have restricted the possible landing configurations such that the goal landing airfoil was not achievable via the given actuation operation. Further configurations not possible during the more restrictive landing

Table 6. Optimized SMA insert lengths (in millimeters).

l_{L1}	l_{L2}	l_{L3}	l_{L4}	l_{L5}	l_{U1}	l_{U2}	l_{U3}	l_{U4}	l_{U5}
10.3	76.1	19.4	10.5	18.6	15.0	64.7	75.3	14.0	11.3

SMA: shape memory alloy.

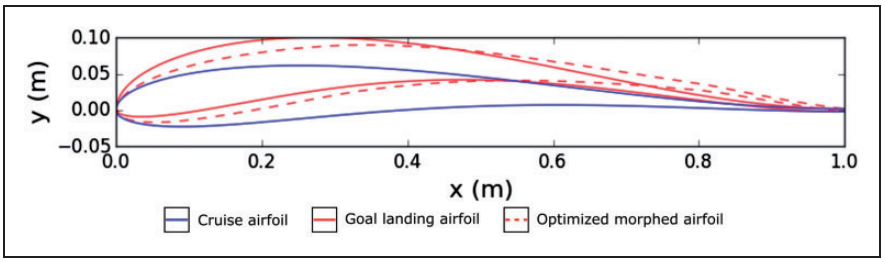

Figure 9. Final calculated airfoil section profiles.

Table 7. Comparison between aerodynamic coefficients for morphed and goal landing airfoil at landing condition where L = W.

	Lift coefficient	Drag coefficient	Landing velocity (m/s)
Landing	1.5588	0.01690	15.00
Morphed	1.6803	0.01832	14.45
Difference	+7.8%	+8.4%	−3.7%

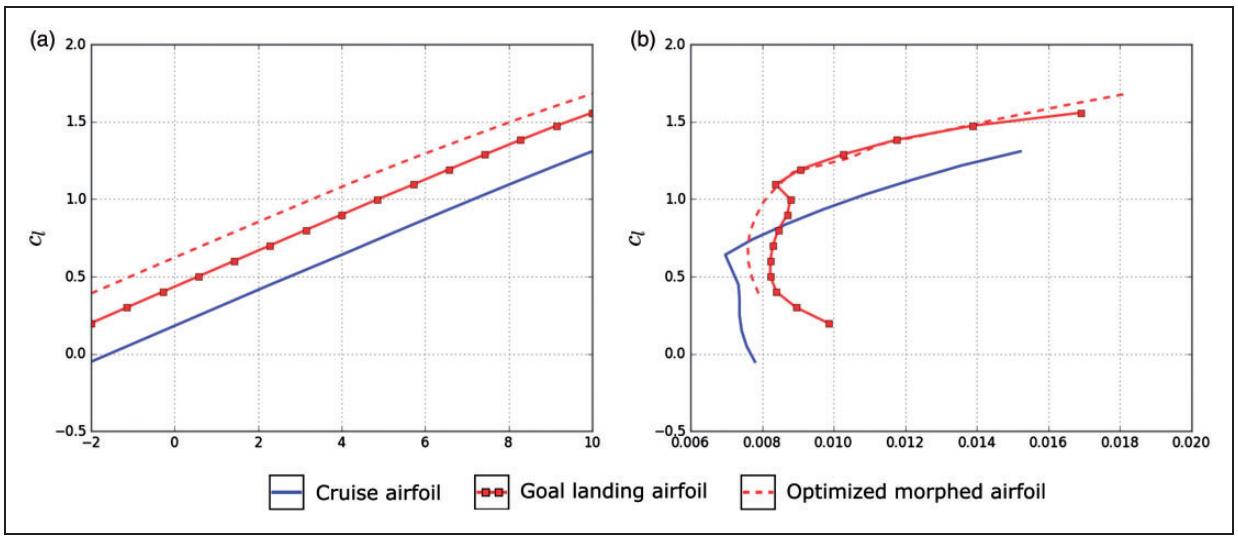

Figure 10. Comparison at landing conditions between approximately optimized cruise, goal landing and obtained landing airfoil. (a) Lift vs. angle of attack and (b) Drag polar.

optimization are possible because of the internal structural deformations computed during morphing analysis. Therefore, although the landing sub-optimization was intended to approximately identify the airfoil section with the lowest landing velocity, the results in Table 7 show that the predicted optimal morphed airfoil provides a slightly better design at 1000 ft and $\alpha = 10^{\circ}$. In case of a failure of the morphing mechanism, the generated lift would be 25% smaller. Therefore, the landing velocity would be increased or other control surfaces would be utilized for a successful landing. Overall, as shown in the plots of Figure 10 and demonstrated in the data of Table 7, the obtained morphing design can successfully modify the cruise airfoil to provide performance similar to that of the goal landing airfoil.

Conclusion

This work introduces a concept for an SMA actuator-driven morphing wing that has heretofore not been considered in detail and an associated design approach in which a number of analysis components (e.g., Abaqus/XFOIL interface for fluid–structure simulation) have been developed and integrated in a single design optimization framework. The approach adopted differs from those of previous works in that the wing design consists of multiple sub-optimizations of the whole structure using coupled fluid–structure analysis. The obtained airfoil for cruise leads to satisfactory performance when compared to existing aircraft benchmarks. Finally, it is demonstrated in analysis that fully integrated design of airfoil and distributed actuators is possible and that SMA-driven reconfigurable wings are structurally feasible against stress and buckling constraints.

Current efforts are now focused on more realistic thermal control by considering different heating methods. The substantial cooling effects of the freestream over skin-mounted actuators are incorporated into this analysis. The associated selection of an approximate control scheme and the use of aerodynamic analysis tools that can better account for stall are also under consideration. Further studies may also include morphing wings for more than two discrete flight conditions as well as prototyping and testing for physical validation of the design herein presented.

Acknowledegments

The technical help of Dr Edwin Peraza Hernandez and Chris Bertagne is also gratefully acknowledged. Structural analysis was performed via an Academic Research license from Simulia. Optimization and tool integration were accomplished via OpenMDAO. Aerodynamic analysis was accomplished via XFOIL. Thanks to Hannah Stroud for proofreading the paper.

Declaration of Conflicting Interests

The author(s) declared no potential conflicts of interest with respect to the research, authorship, and/or publication of this article.

Funding

The author(s) disclosed receipt of the following financial support for the research, authorship, and/or publication of this article: The authors would like to acknowledge the support of the Brazilian Research Agency, CNPq, through the scholarship provided by INCT-EIE (National Institute of Science and Technology—Smart Structures in Engineering) during the stay at Texas A&M University.

References

1. Torenbeek E. *Synthesis of subsonic airplane design*. Dordrecht, The Netherlands: Springer Science & Business Media, 1982.
2. Anderson JD Jr. *Fundamentals of aerodynamics*. 2nd ed. New York: McGraw-Hill, 1991.
3. Valasek J. *Morphing aerospace structures*. Chichester, West Sussex, UK: John Wiley & Sons, 2012.
4. DC Lagoudas (ed.). *Shape memory alloys: modeling and engineering applications*. New York: Springer-Verlag, 2008.
5. Hartl DJ and Lagoudas DC. Aerospace applications of shape memory alloys. *Proc IMechE, Part G: J Aerospace Engineering* 2007; 221(Special Issue): 535–552.
6. Barbarino S, Flores Saavedra EI, Ajaj RM, et al. A review on shape memory alloys with applications to morphing aircraft. *Smart Mater Struct* 2014; 22: 823–877.
7. Joo JJ, Marks CR, Zientarski L, et al. Variable camber compliant wing – design. In: *Proceedings of 23 rd AIAA/AHS adaptive structures conference*, Kissimmee, FL, 5–9 January 2015.
8. Previtali F, Arrieta AF and Ermanni P. Double-walled corrugated structure for bending-stiff anisotropic morphing skins. *J Intell Mater Syst Struct* 2015; 26: 599–613.
9. Yokozeki T, Sugiura A and Hirano Y. Development of variable camber morphing airfoil using corrugated structure. *J Aircraft* 2014; 51: 1023–1029.
10. Icardi U and Ferrero L. Preliminary study of an adaptive wing with shape memory alloy torsion actuators. *Mater Des* 2009; 30: 4200–4210.
11. Francesco Previtali, Tommaso Delpero, Andrea Bergamini, Andres F Arrieta, Paolo Ermanni. Extremely anisotropic multi-functional skin for morphing applications. In: *Proceedings of 23 rd AIAA/AHS adaptive structures conference*, Kissimmee, FL, 5–9 January 2015.
12. Bilgen O, Kochersberger KB, Inman DJ, et al. Novel, bidirectional, variable-camber airfoil via macro-fiber composite actuators. *J Aircraft* 2010; 47: 303–314.
13. Ramrakhyani DS, Lesieutre GA, Frecker MI, et al. Aircraft structural morphing using tendon-actuated compliant cellular trusses. *J Aircraft* 2005; 1614–1620.
14. Ursache NM, Keane AJ and Bressloff NW. Design of postbuckled spinal structures for airfoil camber and shape control. *AIAA J* 2006; 44: 3115–3124.
15. Woods BKS, Dayyani I and Friswell MI. Fluid/structure-interaction analysis of the fish-bone-active-camber morphing concept. *J Aircraft* 2015; 52: 307–319.
16. Airoldi A, Crespi M, Quaranti G, et al. Design of a morphing airfoil with composite chiral structure. *J Aircraft* 2012; 49: 1008–1019.

17. Coutu D, Brailovski V and Terriault P. Promising benefits of an active-extrados morphing laminar wing. *J Aircraft* 2009; 46: 730–731.
18. Xijuan G, Qiang Z and Xi F. Design segmented stiff skin for a morphing wing. *J Aircraft* 2015; 53: 962–970.
19. Calkins FT and Mabe JH. Shape memory alloy based morphing aerostructures. *J Mech Des* 2010; 132: 111012.
20. Dong Y, Boming Z and Jun L. A changeable aerofoil actuated by shape memory alloy springs. *Mat Sci Eng* 2008; 485: 243–250.
21. Strelec JK, Lagoudas DC, Khan MA, et al. Design and implementation of a shape memory alloy actuated reconfigurable wing. *J Intell Mat Syst Struct* 2003; 14: 257–273.
22. Abdullah EJ, Bil C and Watkins S. Testing of adaptive airfoil for UAV using shape memory alloy actuators. In: *Proceedings of 27th international congress of the aeronautical sciences*, Nice, France, 19–24 September 2010.
23. Kudva J. Overview of the DARPA smart wing project. *J Intell Mat Syst Struct* 2004; 15: 261–267.
24. Peel LD, Mejia J, Narvaez B, et al. Development of a simple morphing wing using elastomeric composites as skins and actuators. *J Mech Des* 2009; 131: 091003.
25. Senthilkuma M. Analysis of SMA actuated plain flap wing. *J Eng Sci Tech* 2012; 5: 39–43.
26. Chopra I. *Recent progress on development of a smart rotor system*. Langley, VA: NASA Langley Research Center, 2001.
27. Oehler SD, Hartl DJ, Lopez R, et al. Design optimization and uncertainty analysis of SMA morphing structures. *Smart Mater Struct* 2012; 21: 094016.
28. Junior LCL, Savi MA, Hartl DJ, et al. Morphing airfoil: camber optimization using shape memory alloys. In: *Proceedings of 22nd international congress of mechanical engineering*. Ribeirao Preto, Brazil, 3–7 November 2013.
29. Ma J, Karaman I and Noebe RD. High temperature shape memory alloys. *Int Mat Rev* 2010; 55: 257–315.
30. Santamarta R, Arroyave R, Pons J, et al. TEM study of structural and microstructural characteristics of a precipitate phase in Ni-rich Ni-Ti-Hf and Ni-Ti-Zr shape memory alloys. *Acta Materialia* 2013; 61: 6191–6206.
31. Hartl DJ, Lagoudas DC and Calkins FT. Advanced methods for the analysis, design, and optimization of SMA-based aerostructures. *Smart Mater Struct* 2011; 094006 (20pp).
32. Leal PBC, Bertagne CL and Hartl DJ. Aero-structural optimization of shape memory alloy-based wing morphing via a class/shape transformation approach. In: *Proceedings of 23rd AIAA/AHS adaptive structures conference*, Kissimmee, FL, 5–9 January 2015.
33. Kulfan BM and Bussoletti JE. Fundamental parametric geometry representations for aircraft component shapes. In: *Proceedings of 11th AIAA/ISSMO multidisciplinary analysis and optimization conference*. Portsmouth, Virginia, 6–8 September 2006.
34. Statistical Summary of Commercial Jet Airplane Accidents, Boeing, http://www.boeing.com/resources/boeingdotcom/company/about_bca/pdf/statsum.pdf (1959–2008).
35. Abaqus. *Analysis user's manual*. Woodlands Hills, CA: Author, 2007.
36. XFOIL 6.9 User Primers, MIT AERO and Astro, Harold Youngren, Aerocraft, Incl, http://web.mit.edu/aeroutil_v1.0/xfoil_doc.txt (2001).
37. Lagoudas D, Hartl D, Chemisky Y, et al. Constitutive model for the numerical analysis of phase transformation in polycrystalline shape memory alloys. *Int J Plast* 2012; 32–33: 155–183.
38. Deb K, Pratap A, Agarwal S, et al. A fast and elitist multiobjective genetic algorithm: NSGA-II. *IEEE Trans Evol Comput* 2002; 6: 181–197.
39. Gray JS, Moore KT and Naylor BA. OPENMDAO: An open source framework for multidisciplinary analysis and optimization. In: *Proceedings of 13th AIAA/ISSMO multidisciplinary analysis and optimization conference*, Fort Worth, TX, 13–15 September 2010.
40. Grodzevich O and Romanko O. Normalization and other topics in multi-objective optimization. In: *Proceedings of the Fields-MITACS Industrial Problems Workshop*, Toronto, Canada, 14–18 August 2006.
41. Ishibuchi H, Nojima Y and Doi T. Comparison between single-objective and multi-objective genetic algorithms: performance comparison and performance measures. In: *Proceedings of 2006 IEEE international conference on evolutionary computation*, Vancouver, BC, Canada, 16–21 July 2006.
42. Murugan P, Kannan S and Baskar S. Application of NSGA-II algorithm to single-objective transmission constrained generation expansion planning. *IEEE Trans Power Syst* 2009; 24: 1790–1797.
43. Lane AK and Marshall DD. A surface parameterization method for airfoil optimization and high lift 2D geometries utilizing the CST methodology. *AIAA J* 2009; 1461: 5–8.
44. Bogue D and Crist N. CST transonic optimization using Tranair++. In: *Proceedings of 46th AIAA aerospace sciences meeting and exhibit*. Reno, NV, 7–10 January 2008.
45. Felippa CA, Park KC and Farhat C. Partitioned analysis of coupled mechanical systems. Center for Aerospace Structures. Boulder, Colorado: University of Colorado, 1999.
46. Bertagne C, Moghadas P, Malak R, et al. Feedback control applied to finite element models of morphing structures. In: *Proceedings of ASME 2014 conference on smart materials, adaptive structures and intelligent systems*. Buffalo, NY, 8–10 September 2014.
47. Leal PBC AeroPy: An easy to use aerodynamics tool. Computer software, Version Alpha, 2016.
48. Metallic Materials Properties Development and Standardization (MMPDS-01). U.S. Department of Transportation. Columbus, Ohio: Battelle Memorial Institute, 2012.
49. Saunders R, Hartl D, Malak R, et al. Design and analysis of a self-folding SMA-SMP composite laminate. In: *Proceedings of ASME 2014 international design engineering technical conferences and computers and information in engineering conference*. Buffalo, NY, 17–20 August 2014.
50. Hoffman J, Jansson J and Johnson C. New theory of flight. *J Math Fluid Mech* 2016; 18: 219–241.

51. Taylor M. *Jane's encyclopedia of aviation*. New York, Avenel, NJ: Portland House, 1989.
52. Gere JM and Goodno BJ. *Mechanics of materials*. 8th ed. Stamford, CT: Cengage Learning, 2013.
53. Bryan K and Shibberu Y. *Penalty functions and constrained optimization*. Report, Department of Mathematics, Rose-Hulman Institute of Technology, USA, 2015.
54. Abbott IH and Doenhoff AEV. *Theory of wing sections, including a summary of airfoil data*. Courier Corporation, 1959.
55. Reeves CR. Using genetic algorithms with small populations. In: *Proceedings of the 5th international conference on genetic algorithm*, San Mateo, CA, 17–21 July 1993.
56. Drela M. *Flight vehicle aerodynamics*. Cambridge, MA: The MIT Press, 2014.